



# Experimental and numerical study on the mechanical behavior of Q460D high-strength steel bolted connections

Hongchao Guo <sup>a,b,\*</sup>, Feng Xiao <sup>a,b</sup>, Yunhe Liu <sup>a,c</sup>, Gang Liang <sup>a,b</sup>

<sup>a</sup> State Key Laboratory Base of Eco-hydraulic Engineering in Arid Area, Xi'an University of Technology, No. 5, Jinhua Road, Xi'an 710048, PR China

<sup>b</sup> School of Civil Engineering and Architecture, Xi'an University of Technology, No. 5, Jinhua Road, Xi'an 710048, PR China

<sup>c</sup> Institute of Water Resources and Hydro-electric Engineering, Xi'an University of Technology, No. 5, Jinhua Road, Xi'an 710048, PR China



## ARTICLE INFO

### Article history:

Received 21 April 2018

Received in revised form 19 August 2018

Accepted 12 September 2018

Available online xxxxx

### Keywords:

High strength steel

Bolted connection

Connection construction

Ultimate capacity

Net cross section

## ABSTRACT

Based on static tensile test of 20 Q460D high-strength steel bolted connection joints, influences of high-strength steel material strength and bolt arrangement pattern on bearing capacity and deformation of connections were analyzed. According to differences of end distance, edge distance, and pitch between bolts, finite element modeling, theoretical calculation, and test results were compared, a quantitative analysis was carried out for mechanical property of high-strength steel bolted connections, and applicability of relevant standards was investigated. The study showed that bearing capacity and deformation of specimens for Q460D high-strength steel increased as pitch increased when bolts were under transversal arrangement. Influence of increased edge and end distance on bearing capacity of the connection was minimal after standard value of the structure was reached. Stress nephogram obtained from numerical analysis and plastic region presented symmetrical distribution with two holes bearing balanced stress, fitted curve points were dispersedly distributed, and margin of theoretically calculated value was large when EC3 standard was used. When bolts were under longitudinal arrangement, bearing capacity of the specimens only presented a linearly increasing trend as pitch increased, two holes bore unbalanced stress in stress distribution, stress borne by bolt hole at end part and its deformation were both large, and bearing capacities of end and middle bolts calculated according to the EC3 standard were relatively accurate. This study can provide a theoretical basis for design and connection structure of Q460D high-strength steel bolted connection joints.

© 2018 Elsevier Ltd. All rights reserved.

## 1. Introduction

With the improvement of steel production technology and maturation of corresponding welding materials and connection technology, novel high-strength steel materials have been successfully applied in many buildings globally and favorable social and economic benefits have been achieved [1–4].

Since the late 1960s, partial scholars have carried out a few experimental studies on high-strength steel bolted connections, mainly analyzed influences of bolt pitch and high-strength steel material properties on bearing capacity of connection joints, and discussed the applicability of existing design methods to high-strength steel bolted connection. Wallaert and Fisher [5,6] studied influences, such as bolt pretension, shearing plane position, contact surface roughness, bolt grade, and diameter on shear resistance. Zeynali et al. [7] analyzed influences of different material properties, number of bolts, amount of

frictional coefficient and the type of connections on load-bearing properties of bolted connection. Pavlina [8] estimated yield and tensile strength of steel materials according to steel hardness measurement. Dusicka et al. [9] studied influences of different plate thicknesses and hole diameters on bearing capacity of bolted connection. Moze and Beg [10–12] conducted a test on high-strength steel bolted connections and proposed a correction formula. They also believed that the EC3 standard was very conservative; that is, a high steel grade leads to significant strength loss. Sterling [13] carried out static tensile test of eight groups of bolted butt connection and analyzed influences of bolt pitch and length of bolted connection on bearing capacity and deformation performance of the connection. Shi et al. [14] tested shear resistance of high-strength bolted-pressure-bearing connection joint and analyzed influences of plate thickness, end distance, and tensile strength. They also discussed load-bearing features of short- and long-joint connections. Kim and Kuwamura [15,16] analyzed influences of plate thickness, edge and end distance etc. parametric on the bearing deformation capacity and failure modes by finite element. Puthli and Fleischer [17] analyzed influences of bolt pitch, edge and end distance on load-bearing properties of bolted connection and proposed suggestions for parameter values. Analberg and Larsen [18,19] compared

\* Corresponding author at: School of Civil Engineering and Architecture, Xi'an University of Technology, No. 5, Jinhua Road, Xi'an City, Shan Xi Province 710048, P.R. China

E-mail address: ghc-1209@163.com (H. Guo).

load-bearing properties of high-strength steel and ordinary strength steel bolted connections and found that failure mode of ordinary strength steel was net sectional failure and yield/strength ratio did not have any influence on deformability. Rex and Easterling [20] studied 48 groups of shear-resisting bolted connection specimens when end distance was large and steel plate was thin (6.5 mm), in which pitch between inner plates would gradually become large and finally be drawn away. Hongchao Guo [21,23] conducted experimental study and numerical analysis of Q690D high-strength T-stub connections; analyzed influences of parameters, such as bolt diameter, strength grade, and scale effect of flange plate on failure mode and mechanical properties of the joints; and proposed a computational formula of T-stub joint original rigidity considering bending deformation of bolts.

In general, on the one hand, the mechanical properties of bolted joints are mostly concentrated in ordinary steel. There are relatively few tests on the connection of HSS with a yield strength of more than 420 MPa, so there is a lack of support for a large number of basic test data. On the other hand, EC3, ANSI specifications, etc. allow the high-strength steel of 690 MPa strength grade to be applied in engineering, but all adopt the unified formulas, and only in some aspects, the reduction coefficients are used to consider the deficiency of toughness and ductility of HSS as well as the material strength fluctuation factor, which lack the background research work and results of HSS.

Compared with ordinary steel, high-strength steel has high yield strength (close to the strength of high-strength bolt) and poor plasticity [25,26]. Problems in bolted connection, such as material matching attribute, failure mode, and plastic deformation capability, constitute the focus of this study. While connection strength is ensured, the joints should have certain deformation capabilities to allow stress redistribution of connecting steel plates. This paper carried out an experimental study of load-bearing properties of Q460D high-strength steel bolted connections under longitudinal and transverse arrangements and then analyzed influences of different bolt arrangement patterns and their pitch on bearing capacity of bolted connections. A comparison with theoretically calculated values was carried out through GB50017, EC3, and ANSI [27–29], the applicability of existing standard computational formula was discussed, and construction suggestions applicable to high-strength steel bolted connections were provided. The present study provided a scientific basis for design theory and method of high-strength structural steel bolted connections.

## 2. Experimental program

### 2.1. Specimen design

Two groups of high-strength steel bolted shear-resisting connection specimens were designed in this experiment, and steel plates were connected through high-strength bolts. Group A comprised Q460D bolts under transverse arrangement, while group B comprised Q460D bolts under longitudinal arrangement to investigate the influence of bolt arrangement pattern on load-bearing properties of connections. Cover and inner plates in the test were Q460D rolled steel with thickness of

8 mm, and high-strength bolt was 10.9 grade M20 with hole diameter  $d_0$  of 22 mm.

A torque wrench was used to apply pretension to high-strength bolts. According to stipulations in *Technical Specification for High-Strength Bolt Connections of Steel Structures* [30], final screw torque of high-strength construction bolts was determined to 510 N·m, and bolts were individually tightened along the middle part toward the two ends. Main parameters of the connection were end distance  $e_1$ , edge distance  $e_2$ , and bolt pitch  $p_2$ ;  $e_1 \geq 2.0d_0$ ,  $e_2 \geq 1.5d_0$ , and  $p_2 \geq 3.0d_0$  were stipulated in the *Code for Design of Steel Structure* (GB50017-2017). Geometric dimensions of the specimens are shown in Fig. 1 and Table 1, and Q460D material test results are presented in Tables 2 and 3.

### 2.2. Material properties

Material testing was implemented according to relevant stipulations of *Metallic materials – Tensile Testing at Ambient Temperature* (GB/T228-2002) and *Steel and Steel Products – Location and Preparation of Test Pieces for Mechanical Testing* (GB/T2975-1998) [31,32], and main material property parameters were presented in Tables 2 and 3.

### 2.3. Test setup and loading procedure

A 50 t MTS testing machine was used for the tensile test of connection joints, and loading device and instrument arrangement are presented in Fig. 2. The loading process was carried out through the method stipulated in *Metallic Materials – Tensile Testing – Part 1: Method of Test at Room Temperature* (GB/T 228.1-2010) [33]. Before the test, we first preloaded to 5 kN and then unloaded to zero. The test was formally started after instruments and loading devices were under normal operation through examination and loading rate was 1 kN/s. A vernier caliper was used to measure actual dimensions of the specimens. Displacement and strain data were recorded by TDS-303 acquisition equipment, and force and displacement applied by an actuator would be recorded by MTS servo loading system.

## 3. Finite element analysis

### 3.1. Finite element models

Using abaqus for analysis, inner plates, cover plates, and bolts were all C3D8R solid elements, and components were put under shape regularization treatment before meshing operation. Methods, such as addition of several locally arranged seeds and segmentation of irregular regions, were used for local subdivision of the meshes to improve computational accuracy in open-hole region. The finite element model is shown in Fig. 3, reference points RP-1 and RP-2 were established 20 mm away from the loading center, coupling constraints were set between loading surface and reference points, loading force was applied on reference points, and concentrated forces were uniformly distributed on stress surface.

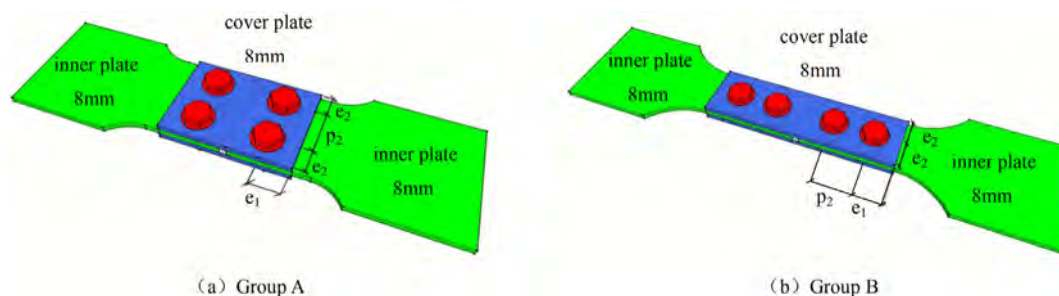


Fig. 1. Layout of specimen.

**Table 1**  
Parameters of specimens.

Specimen number	Bolt characteristics	Steel grade	$t$	$e1$	$e2$	$p2$	Specimen number	Bolt characteristics	Steel grade	$t$	$e1$	$e2$	$p2$
			mm	mm	mm	mm				mm	mm	mm	mm
A1	10.9,M20	Q460D	8	44	33	77	B1	10.9,M20	Q460D	8	44	33	77
A2	10.9,M20	Q460D	8	44	33	66	B2	10.9,M20	Q460D	8	44	33	66
A3	10.9,M20	Q460D	8	44	33	55	B3	10.9,M20	Q460D	8	44	33	55
A4	10.9,M20	Q460D	8	44	33	44	B4	10.9,M20	Q460D	8	44	33	44
A5	10.9,M20	Q460D	8	44	44	66	B5	10.9,M20	Q460D	8	44	44	66
A6	10.9,M20	Q460D	8	44	26.4	66	B6	10.9,M20	Q460D	8	44	26.4	66
A7	10.9,M20	Q460D	8	44	22	66	B7	10.9,M20	Q460D	8	44	22	66
A8	10.9,M20	Q460D	8	55	33	66	B8	10.9,M20	Q460D	8	55	33	66
A9	10.9,M20	Q460D	8	33	33	66	B9	10.9,M20	Q460D	8	33	33	66
A10	10.9,M20	Q460D	8	22	33	66	B10	10.9,M20	Q460D	8	22	33	66

### 3.2. Contact simulation

Contact between components mainly included three parts: contact between nut and cover plate surface, contact between screw and inner side of hole wall in connecting plate as well as the contact between cover and connecting plate surface. Detailed contact relations are presented in Fig. 3. Contact attribute definition was mainly divided into two types: “tangential contact” and “normal contact.” The former was defined by Coulomb frictional force, in which tangential contact between cover and connecting plate and that between nut and cover plate were both frictional forces, and friction coefficient was taken as 0.25 according to Literature [11]. The latter was set as “hard contact,” which allowed separation after contact. “Tangential contact” between bolt rod and the inner side of hole wall was defined as friction-free contact. Disregarding friction between bolt rod and hole wall, contact surface load was transferred by steel plate in a pressure-bearing way to mainly simulate mutual thrust between bolt rod and connecting plate. All contacts were “surface-to-surface contacts.” Selection of principal and subordinate surfaces was determined by mesh density, “normal contact” was defined as “linear,” and contact stiffness was taken as  $2000 \text{ N}\cdot\text{mm}^{-1}$  [36] through repeated computation to improve convergence and computational efficiency.

### 3.3. Material modeling

Engineering stress–strain relation obtained through conversion of load–displacement curves in material test could not accurately express real mechanical behaviors of materials, especially under large strain. Moreover, the fracture section after material necking would continuously reduce, which would influence the determination of real stress–strain relation. Engineering stress–strain relation was corrected through the following equations to obtain the real stress–strain relation as:

$$\sigma_n = \sigma(1 + \varepsilon), \quad (1)$$

$$\varepsilon_n = \ln(1 + \varepsilon), \quad (2)$$

where  $\sigma$  and  $\varepsilon$  are engineering stress and strain, respectively, and  $\sigma_n$  and  $\varepsilon_n$  are real stress and strain, respectively.

In finite element analysis, material plastic behaviors were simulated through a multi-segment linear model which replaced real steel stress–strain curves, as shown in Fig. 4. Constitutive relation of high-strength bolts was expressed by a double broken-line elastic–plastic constitutive

model (as shown in Fig. 5), and main data are presented in Table 3. All materials were isotropic, Poisson's ratios were all taken as 0.3, and von Mises yield criterion was used.

### 3.4. Solving setting

The analytical and computational process was divided into the following three load steps: First, all degrees of freedom at nodes of upper and lower bolt end planes were constrained to steadily establish contact relations. Second, corresponding pretension values were applied to high-strength bolts. Third, displacement load was applied to reference points RP-1 and RP-2 to uniformly distribute concentrated forces on the stress surface. Displacement was used for loading control, and maximum displacement was 20 mm. Owing to the nonlinearity of the computational model, each load step was taken as 5% of total displacement. Full Newton–Raphson method was used for iterative computation.

## 4. Experimental and finite element analysis results

### 4.1. General behavior

Load–displacement curves of group A specimens are shown in Fig. 6, and specimen A2 was designed according to standard construction dimensions. In initial loading stage, horizontal load was mainly transferred by frictional force between contact surfaces of steel plates, curves presented a linear growth trend, and slopes were identical. Bolt rod and hole wall closely contacted each other with the occurrence of horizontal slippage under a gradually increasing load. Afterward, extrusion force was generated by plates, curve slope slowed down, and pressure bearing of bolt steel plate and shear resistance jointly bore horizontal load. Moreover, horizontal displacement increment of the specimen was obviously larger than that in the later stage. After peak load was reached, specimen bearing capacity no longer increased while horizontal displacement abruptly increased, long parallel segments appeared in the curves, and bearing capacity was finally lost due to excessive deformation. All specimens experienced four stages: friction, slippage, pressure bearing, and failure. Maximum slippage did not exceed 2 mm, and all specimens already yielded when deformation value was  $d_0/6$ . Yield platform was long, and bolted connections showed favorable ductility.

Laws of load–displacement curves of group B specimens were similar with those of group A. Owing to the influence of bolt arrangement pattern, horizontal slippage of group B specimens was slightly larger

**Table 2**  
Mechanical properties of the steels.

Steel grade	Plate Thickness	Yield stress	Ultimate stress	Elastic modulus	Yield strength ratio	Tensile elongation
	$t$ (mm)	$f_y$ (MPa)	$f_u$ (MPa)	$E$ (GPa)		$\delta$ (%)
Q460D	8	504.87	591.97	252.43	0.85	25.30

**Table 3**  
Characteristic values of high-strength bolts.

Steel grade	Yield stress $f_y$ (MPa)	Ultimate stress $f_u$ (MPa)
10.9s	900	1000

than that of group A specimens. Owing to the small net cross-sectional area, several specimens failed in net cross-section, net cross-section capacity was within 150–250 kN, which is mostly net cross-sectional failure. Ultimate bearing capacity of bolt specimens under transverse arrangement was obviously larger than that of bolt specimens under longitudinal arrangement.

#### 4.2. Failure modes

Failure modes of specimens varied from geometric parameters, as shown in Fig. 7.

When  $(p_2 + 2e_2)/d_0 \geq 6$  and  $e_1/d_0 \geq 1.5$ , pre-hole thrust failure as in Fig. 7a occurred in A1, A2, A5, A8, and A9, and connecting plate bore screw extrusion force to allow thrust deformation to generate rolled steel near the hole. If  $e_1/d_0 < 1.5$ , then pre-hole thrust failure gradually developed toward end tear-out failure as end distance reduced. End distances among A8, A2, A9, and A10 progressively decreased, A10 experienced oblique cracks  $45^\circ$  of the bolt hole and edge of free end, thus resulting in tear-out failure. Pre-hole plastic deformation before failure was evident, as shown in Fig. 7b. Mixed failure of pre-hole thrust and transverse tear occurred in A7, as shown in Fig. 7c. Presently,  $(p_2 + 2e_2)/d_0 < 6$ ,  $e_1/d_0 \geq 1.5$ , and  $2e_2/p_2 = 2/3$ . When edge distance was small, cracks were initially generated by transverse tensile stress, transverse tear occurred in the hole edge, and maximum principal stress presented hole edge and pre-hole distribution. When  $(p_2 + 2e_2)/d_0 < 6$  and  $e_1/d_0 \geq 1.5$ , net cross-section failure of steel plate occurred in A3, A4, and A6, and pre-hole plastic deformation before failure was small with poor ductility. Group B bolts were under longitudinal arrangement, and effective sectional widths were all smaller than those in group A specimens. End bolts close to the loading end bore large stress. Evident necking phenomenon occurred near bolt holes, during which pre-hole plastic deformation was small, that is, net cross-section failure.

#### 4.3. Theoretical analysis (curves)

The theoretical analysis assumes that slip has occurred at the joints, and the bolts and plates are completely in the pressure state for object

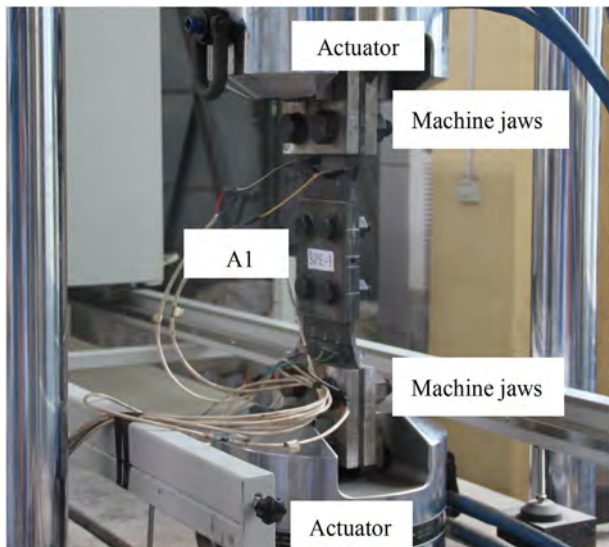


Fig. 2. Test set up.

deployment analysis, ignoring frictional resistance. Bolted connection joint taken as statically indeterminate structure, equation was established according to force equilibrium and deformation coordinating conditions [34].

Force equilibrium condition:

$$P_G - \sum_{i=1}^n R_i = 0. \quad (3)$$

Deformation coordinating condition:

$$\Delta_i + e'_{i,i+1} = \Delta_{i+1} + e_{i,i+1}. \quad (4)$$

where  $P_G$  is the entire load,  $\sum_{i=1}^n R_i$  is the load transferred by all bolts,  $\Delta_i$  and  $\Delta_{i+1}$  are deformations of the  $i$  (th) and  $i + 1$  (th) bolts, respectively, and  $e_{i, i+1}$  and  $e'_{i, i+1}$  are connecting and cover plate deformations, respectively.

The preceding equation shows that bearing capacity and deformation of bolted connection joints can be solved through load–deformation relations among inner plate, cover plate, and bolt. In the elastic stage, average deformation between holes can be expressed as:

$$\varepsilon = \frac{e}{p_2} = \frac{P}{AE}, \quad (5)$$

where  $e$  is the elongation between centers of neighboring holes. For connecting plate,  $P$  is the load borne by a single-pitch connecting plate; for cover plate,  $P$  is the load borne by a single-pitch cover plate.  $A$  is the gross sectional area.

After the minimum section of steel plate reaches yield, stress–strain relation can be expressed as:

$$\sigma = f_y + (f_u - f_y) \left\{ 1 - e^{-\left(\frac{g}{g-d_0}\right) \left(\frac{e}{p_2}\right)^{\frac{3}{2}}} \right\}, \quad (6)$$

where  $g$  is bolt pitch, and  $e_{-}$  is Napierian base.

Taking standard structure specimens A2 and B2 as examples, connecting plate deformation in the elastic stage is as follows:

$$e_1 = \frac{P}{2019.44}. \quad (7)$$

Deformation of connecting plate after yield is.

$$e_1 = 0.088 + \left[ -0.505 \ln \left( 1 - \frac{p-177.714}{30.659} \right)^{\frac{2}{5}} \right], \quad (8)$$

Cover plate and bolt only experience deformation in the elastic stage, and their corresponding formulas are as follows:

Cover plate:

$$e_2 = \frac{P}{4038.88}. \quad (9)$$

Bolt:

$$e_3 = \frac{P}{1680}. \quad (10)$$

Total deformation between the hole centers of connecting and cover plate is  $H$  and  $H = e_1 + e_2 + e_3$ . Test results and theoretical analysis results are shown in Fig. 8. The figure shows that change rules of test curves were similar to those of theoretical analysis curves, and difference between initial spillage load obtained through theoretical calculation and test value did not reach 4%. Moreover, ultimate bearing capacity of specimen B2 increased by 14.9% compared with theoretical value while that of A2 only increased by 8.0%. These results show that

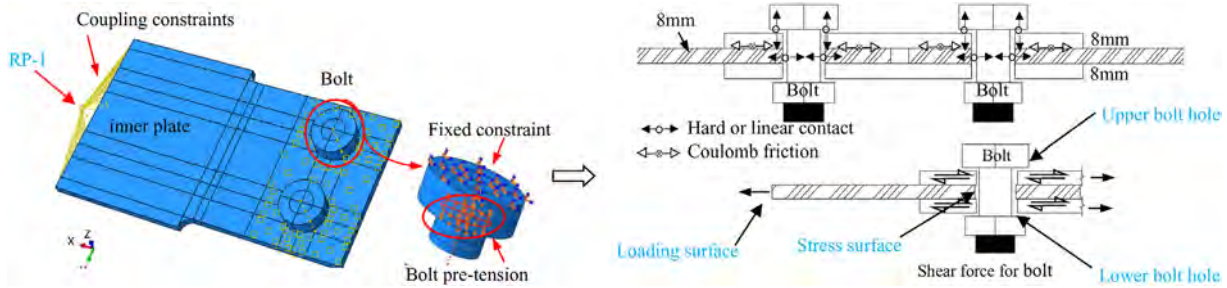


Fig. 3. Contact of high-strength bolt connection.

the method has high precision in calculating the initial sliding load of Q460D high-strength steel bolted connection.

4.4. Load displacement curve

Table 4 provides a comparison of bearing capacities and deformation values obtained through test and finite element analysis value of all specimens in different stages. Owing to the space limitations in this paper, No. 2, 5, and 10 specimens in groups A and B were selected for analysis, and a study by Moze [10] indicated that the specimens experienced yield and connection stiffness started to reduce when deformation value of bolted connection was  $d_0/6$ . Fig. 9 shows that bearing capacities of all specimens were >85% of ultimate bearing capacity when specimen deformation was  $d_0/6$ , and taking  $d_0/6$  deformation value as analysis standard of connection bearing capacity was relatively reasonable. The specimens experienced four stages: friction, slippage, pressure bearing, and failure. Slippage was generated by gaps between bolts and hole walls, finite element analysis was in the ideal state, and was no slippage segment occurred in the simulated load-displacement curves. Slippage was omitted in the analysis process, connection stiffness and bearing capacity of the specimens evidently relatively accorded with test results. The difference value between the test and numerical analysis was within 10%; therefore, the accuracy was quite high.

4.5. Stress distribution

Stress distribution of specimen A2 in the stages is shown in Fig. 10, from which it could be derived that pre-hole stress was large when deformation was  $d_0/18$ . The stress gradually diffused peripherally as the load increased. When deformation was  $d_0/6$ , the stress concentration phenomenon in the pre-hole 10 mm region was evident, maximum stress was approximately 560 MPa, and a few inner plates entered the plastic stage. When deformation was  $d_0/2$ , peak stresses near  $H_1$

and  $H_2$  bolt holes were close to those under  $d_0/6$  at 640 MPa. However, the yield region was obviously enlarged, the transverse part along the hole center was cut through, bolt holes were evidently elongated, and stresses of specimens under transverse arrangement presented symmetric distribution along the centerline of distances between holes.

Net cross-section failure occurred to specimen B2 at end bolt hole  $H_1$ . Maximum stress at end bolt hole edge was approximately 280 MPa under elastic state when deformation was  $d_0/18$ . The peripheral region of end bolt hole  $H_1$  started yielding with a maximum stress of approximately 490 MPa and 130 MPa for inner bolt hole  $H_2$  when deformation was  $d_0/6$ . Maximum stress in the peripheral region of end bolt hole was approximately 604 MPa when deformation was  $d_0/3$ , and two principal stresses were generated along the pre-hole 45° direction. Trajectory direction of principal stresses was identical with maximum shear stress, connecting plate entered the plastic stage along the transverse full section, maximum stress before the inner bolt hole was approximately 160 MPa with small stress, and connecting plate remained in the elastic stage (Fig. 11).

4.6. Deformation analysis

Fig. 12 shows that failure modes obtained through finite element simulation coincided with the test very well, pre-hole thrust failure occurred in specimen A2, computed displacement under the peak load effect was 10.48 mm, test value was 11.64 mm, difference value of displacement was caused by gaps between bolt rod and hole wall in the test, and yield region was within 20 mm scope surrounding the bolt hole. Fig. 13 shows that maximum displacement through finite element modeling of specimen B2 was 8.48 mm and test value was 8.42 mm. Evident necking deformation occurred around end bolt holes, and peripheral steel surrounding inner bolt holes was still

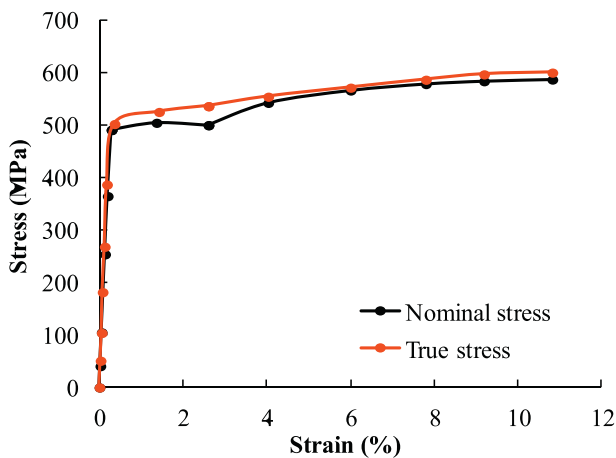


Fig. 4. Stress-strain curves of steels.

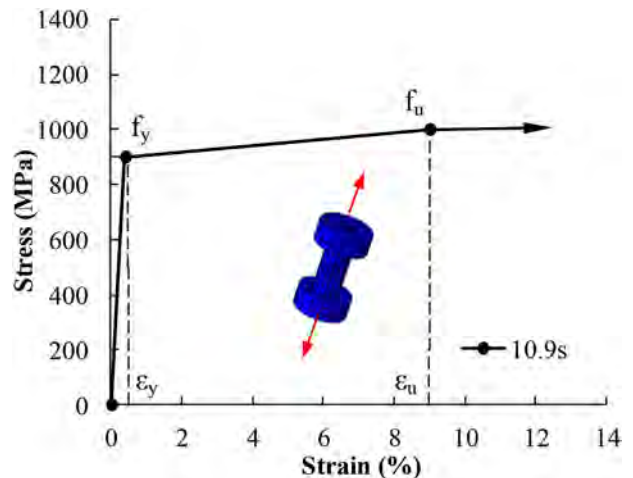


Fig. 5. Stress-strain curves of high strength bolts.

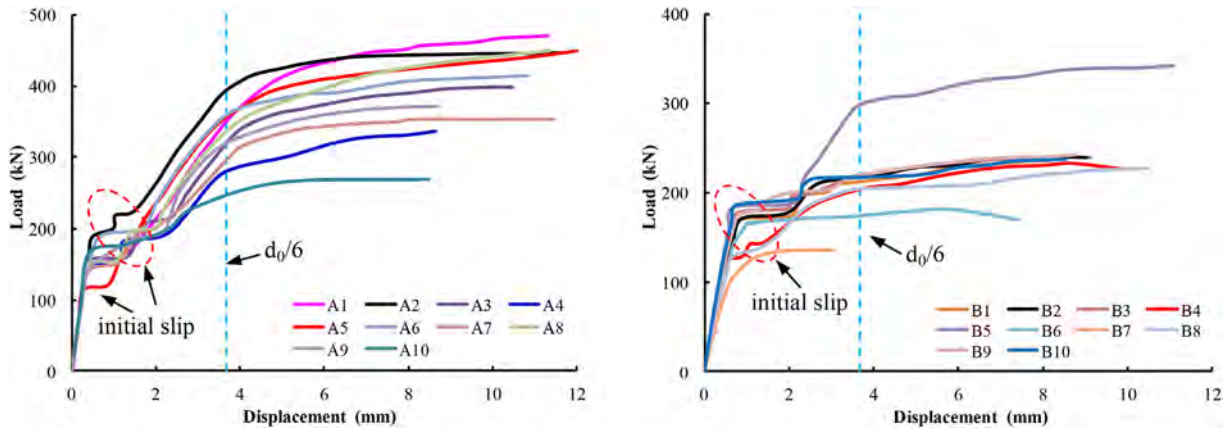


Fig. 6. Load displacement curves.

under the elastic state. In addition, the stress borne by end bolt was far larger than that of inner bolt, and net cross-section failure of steel plate occurred at end bolt, which was identical with the test result.

4.7. Bolt stress analysis

Stresses of group A specimens presented symmetric distribution, contact stresses of bolts B<sub>1</sub> and B<sub>2</sub> were identical, and stresses in the

pre-hole region presented an elliptical distribution. Owing to differences between end bolt and central bolt in stress-bearing in group B specimens, a significant difference existed in bolt stress distributions. Fig. 14a shows that friction force had a certain influence on connection joint bearing capacity, and two bolts in group B specimens bore uneven stresses. Fig. 14c shows that deformation and stress value of end bolt holes were large and bolt rod stresses presented a non-uniform distribution.

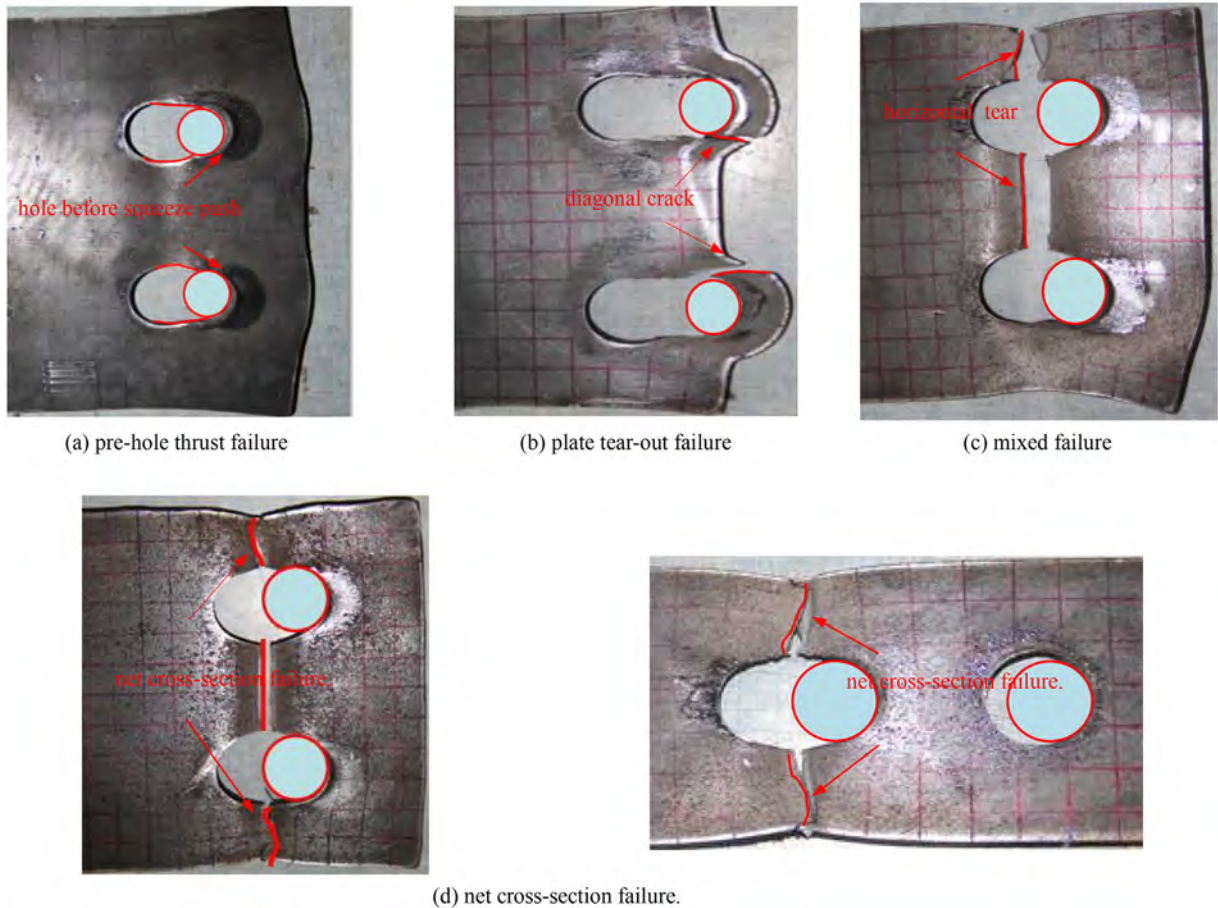


Fig. 7. Failure modes.

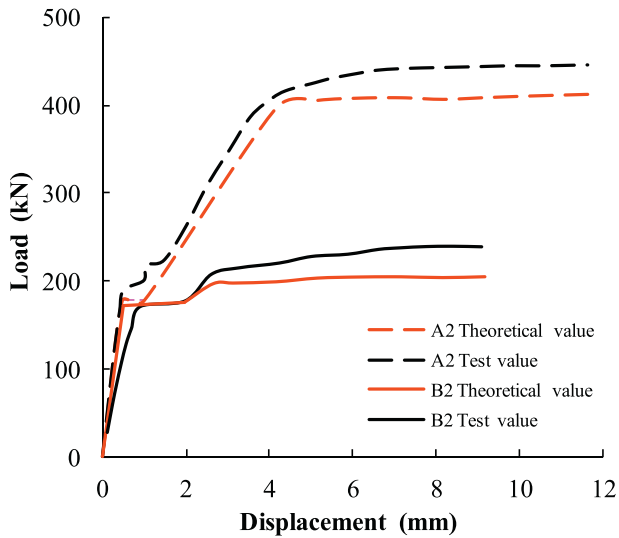


Fig. 8. Comparison of experimental and analytic values.

## 5. Parametric analysis

### 5.1. Bolt end distance

Relation curves of specimen-bearing capacity change with end distance are shown in Fig. 15. When bolts were under transverse arrangement, specimen bearing capacity increased as end distance increased, end distance reduced from  $2.5d_0$  to  $d_0$ , and ultimate bearing capacities reduced by 4.5%, 19.5%, and 35.7%. When  $e_1 > 2d_0$ , amplitude increase of ultimate bearing capacity was relatively small. When bolts were under longitudinal arrangement, change of specimen-bearing capacity with end distance was minor and change amplitude of bearing capacity did not exceed 3%. This finding showed that influence of end distance on longitudinal bolt arrangement was relatively minor.

In different standards, influences of end distance on load-bearing capacities are shown in Fig. 15c:

#### 1) EC3 standard

When  $e_1 < 3d_0$ :

$$\frac{F_b}{f_u dt} = 0.8 \frac{e_1}{3d_0} \left( 2.8 \frac{e_2}{d_0} - 1.7 \right). \quad (11)$$

#### 2) ANSI standard

$$\frac{F_b}{f_u dt} = \varphi 1.2 \frac{e_1}{d} = 0.9 \frac{e_1 d_0}{d_0 d} = 0.99 \frac{e_1}{d_0} \leq \varphi 2.4 = 1.8. \quad (12)$$

Solid data in Fig. 15c are bolts under transverse arrangement and hollow data are bolts under longitudinal arrangement. The figure shows that the influence of end distance on bearing capacity is related to edge distance. When bolts are under transverse arrangement, specimen bearing capacity and end distance present linear growth, and the fitting trend of the ANSI standard is quite approximate while that of the EC3 standard is partially conservative. When bolts are under longitudinal arrangement, end distance nearly does not have any influence on bearing capacity. At present, the EC3 standard has the most favorable fitting effect.

End distance was determined according to the larger steel plate shear resistance than the load transferred by the bolt rod to prevent connections from end tear-out failure. The load transferred by a single bolt is.

$$P_1 = P/2 = f_c dt. \quad (13)$$

The end shear strength of steel plate is

$$P_2 = 2t(e_1 - d_0/2)f_v. \quad (14)$$

Table 4  
The feature point of Load-displacement curve.

Specimen number	Bearing stage (kN)				Peak stage (kN)				Displacement $d_0/6$ (kN)		$(F_{U,FEM} - F_{U,Exp}) / F_{U,Exp}$ (%)	$(\Delta_{U,FEM} - \Delta_{U,Exp}) / \Delta_{U,Exp}$ (%)
	$F_{R,Exp}$	$F_{R,FEM}$	$\Delta_{R,Exp}$	$\Delta_{R,FEM}$	$F_{U,Exp}$	$F_{U,FEM}$	$\Delta_{U,Exp}$	$\Delta_{U,FEM}$	$F_{Exp}$	$F_{FEM}$		
A1	157.06	208.31	1.15	1.47	469.71	484.89	11.32	12.52	360.21	422.65	3.23	10.60
A2	223.20	233.37	1.47	1.67	446.00	476.47	11.64	10.48	386.97	404.48	6.83	9.96
A3	247.31	262.14	2.73	1.75	398.38	410.22	10.48	9.54	338.22	356.11	2.97	8.97
A4	194.18	208.61	2.31	2.34	335.80	338.08	8.64	6.58	284.72	304.29	0.68	23.84
A5	156.74	207.47	1.35	1.27	449.48	477.26	12.26	11.77	350.82	410.59	6.18	4.00
A6	199.74	259.42	1.67	1.85	413.61	403.01	10.85	9.38	364.00	369.63	2.56	13.55
A7	191.33	265.49	2.51	2.92	353.64	362.49	9.13	8.11	225.03	297.45	2.50	11.17
A8	200.07	316.77	2.51	2.31	449.79	490.85	11.88	8.48	288.83	377.04	9.13	28.62
A9	196.39	296.96	2.69	2.01	370.75	363.50	9.21	10.49	292.03	339.06	1.96	13.90
A10	177.86	200.82	1.29	1.62	269.23	256.40	8.18	9.75	264.57	235.21	4.77	19.19
B1	173.15	207.71	2.03	1.87	235.59	240.37	8.21	8.85	211.36	222.81	2.03	7.80
B2	177.07	199.44	1.97	1.31	239.36	252.03	8.42	8.48	217.74	229.15	5.29	0.71
B3	199.49	207.67	2.56	1.76	238.56	240.83	8.09	8.75	214.49	223.24	0.95	8.16
B4	145.04	207.64	2.42	1.86	232.49	240.66	10.11	8.85	179.19	223.25	3.51	12.46
B5	215.84	294.77	2.35	2.11	342.35	354.93	11.09	11.87	280.17	317.25	3.67	7.03
B6	165.30	141.49	1.01	1.21	180.53	171.04	5.85	6.38	172.38	160.36	5.26	9.06
B7	126.13	115.48	1.16	1.31	135.55	134.83	4.05	4.95	130.54	127.11	0.53	22.22
B8	137.31	202.78	1.27	1.66	226.42	240.37	10.47	8.92	203.56	222.53	6.16	14.80
B9	185.77	207.86	1.31	1.96	242.84	240.32	8.75	8.95	217.77	222.36	1.04	2.29
B10	192.55	212.36	2.17	1.72	237.01	251.36	8.53	9.48	221.64	227.74	6.05	11.14

Notes:  $F_R$ -Bearing capacity value at bearing stage;  $F_U$ -Peak value at peak stage;  $\Delta$ -Displacement value of specimen;  $Exp$ -Test value;  $FEM$ -Finite element analysis value.

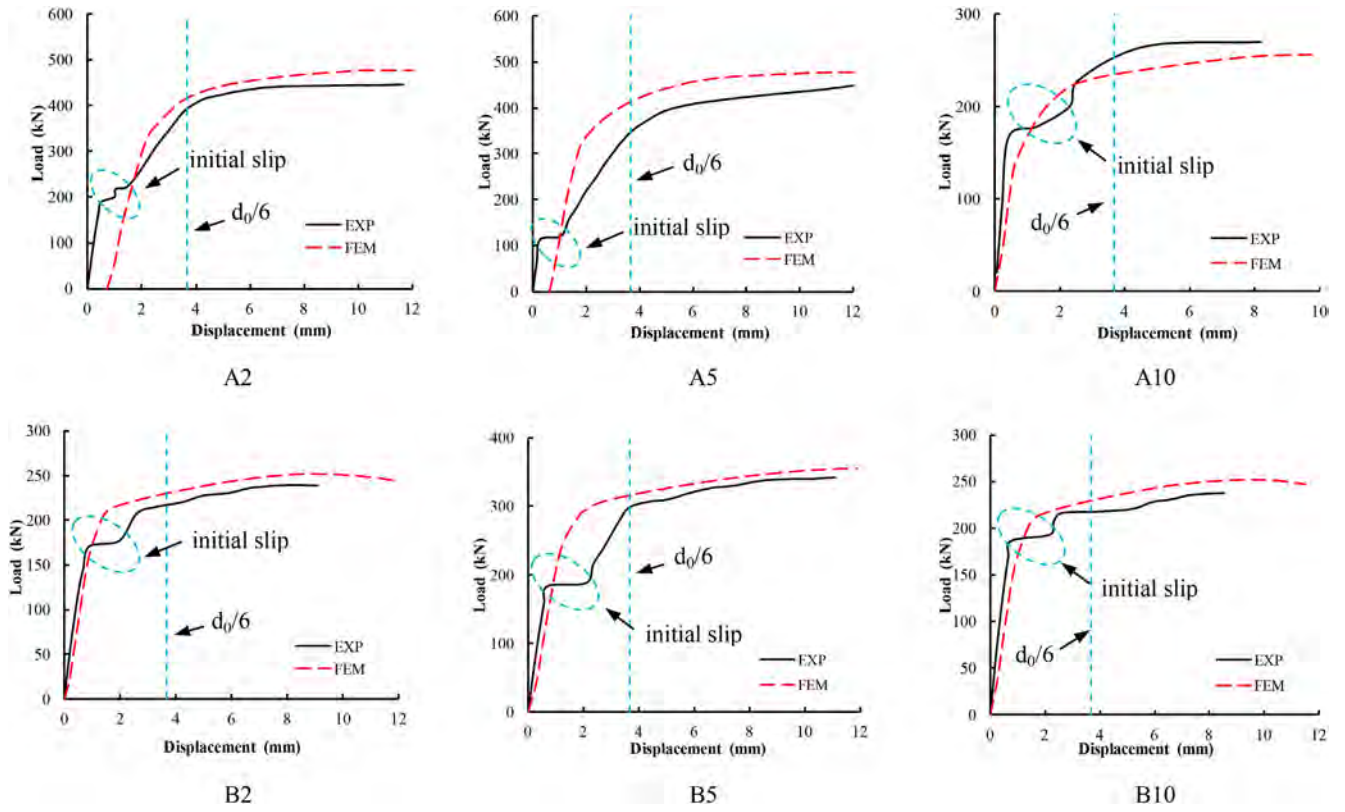


Fig. 9. The comparison of finite element and experimental load displacement curve.

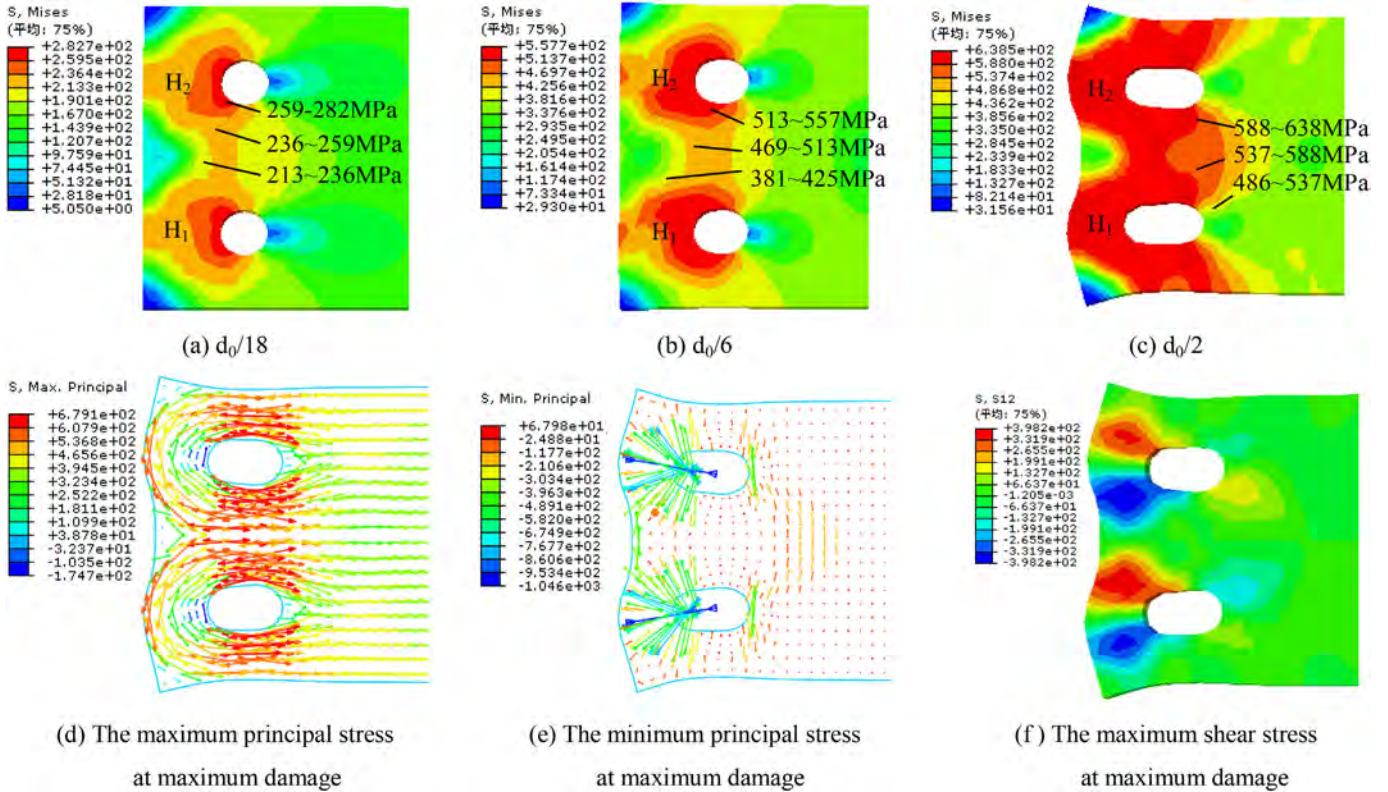


Fig. 10. Stress states of the specimen A2.

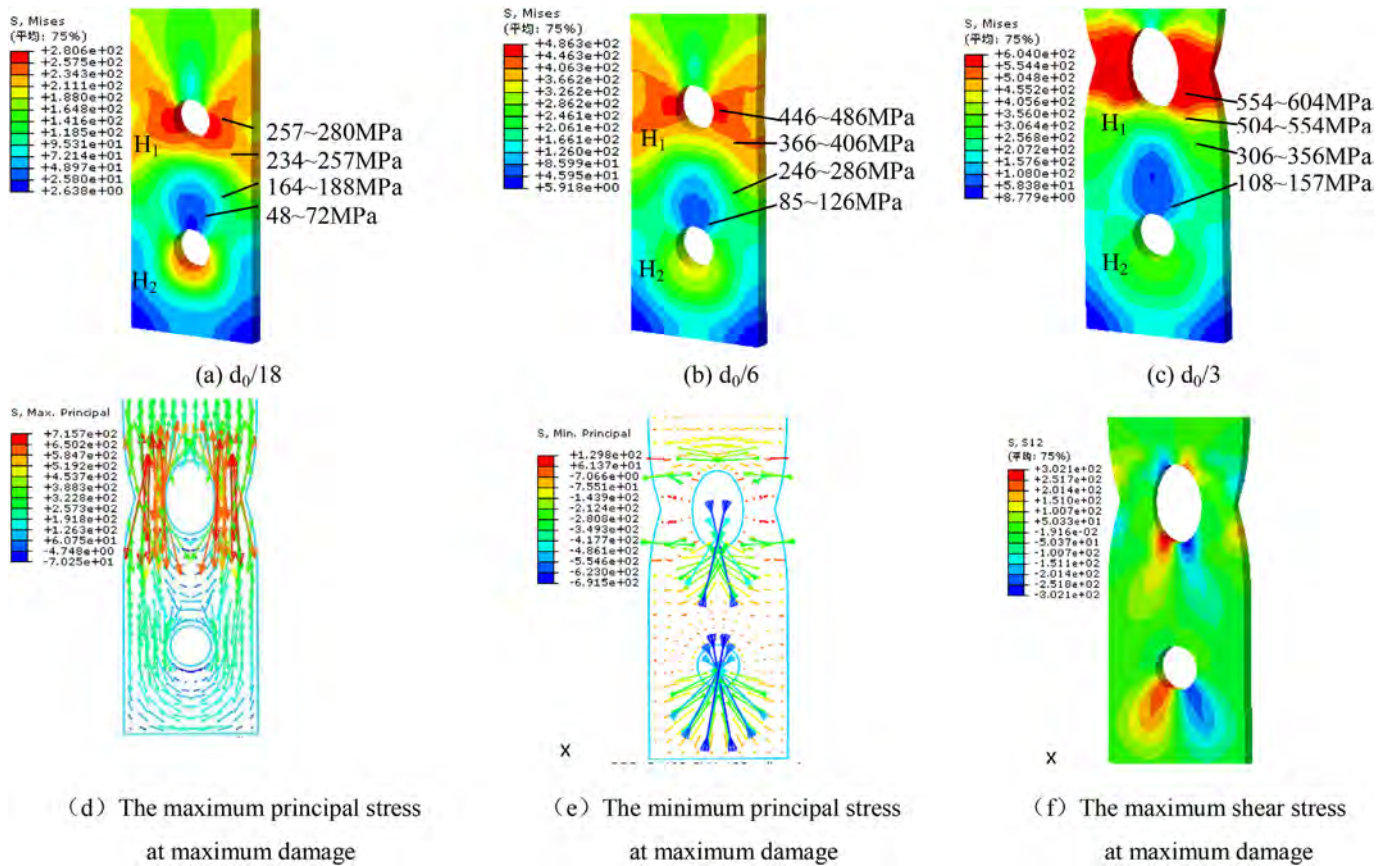


Fig. 11. Stress states of the specimen B2.

where  $f_v$  is steel plate shear strength which is taken as  $1/\sqrt{3}$  of tensile strength, and  $f_c$  is hole of wall bearing stress.

$P_1 \leq P_2$  is assumed as  $d$  is quite close to  $d_0$ , considered as approximately equal for the convenience of computation, and then

$$\frac{f_c}{f_u} \leq 1.155 \frac{e_1}{d_0} - 0.577. \quad (15)$$

Test  $f_c/f_u$  value is 1.67, and  $e_1/d_0 \geq 1.94$  is obtained; therefore, the distance of Q460D bolted joints is suggested as  $2d_0$ .

Relation curves between end distance and bearing strength are shown in Fig. 16, which proves that using Eq. (15) for Q460D bolted

joints is inaccurate; therefore, a correction is needed.

$$\frac{f_c}{f_u} \leq 1.058 \frac{e_1}{d_0} + 0.383. \quad (16)$$

For design value of hole wall bearing strength, 0.7 safety coefficient  $\varphi$  is considered:

$$f_c^b = \varphi f_c = \varphi \left( 1.058 \frac{e_1}{d_0} + 0.383 \right) f_u. \quad (17)$$

As suggested, end distance value is  $2d_0$ ;  $f_c^b = 1.7f_u$  is obtained after the value is substituted into Eq. (17).

Therefore, design value of hole wall bearing strength of Q460D bolted joint was suggested as  $1.7f_u$ , which was relatively higher than

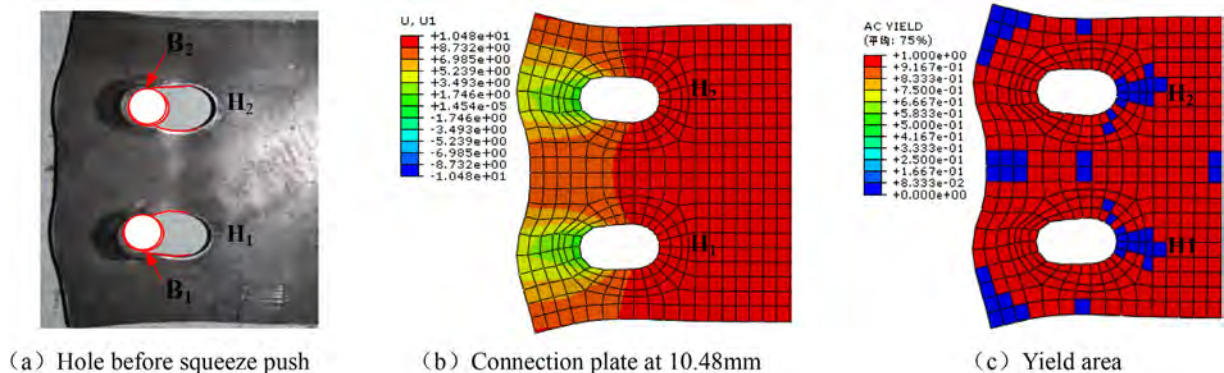


Fig. 12. Deformation damage of the specimen A2.

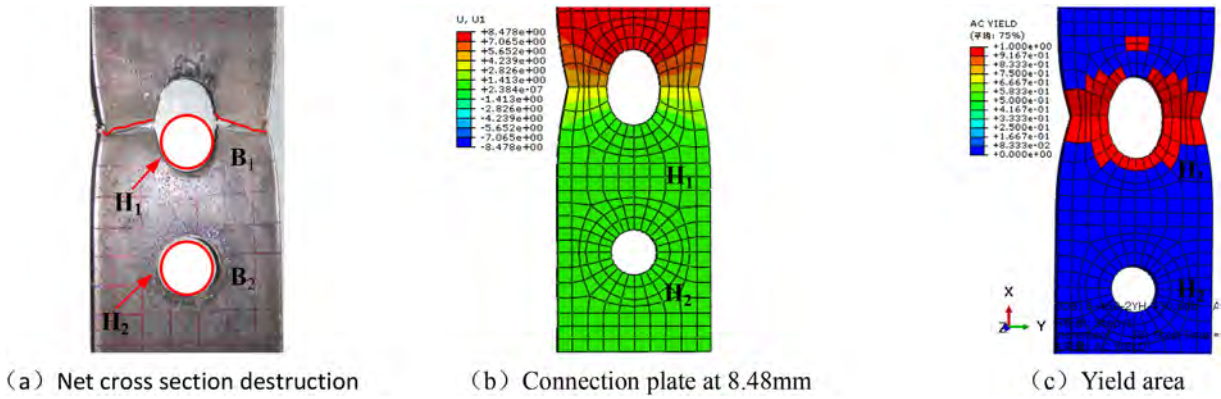


Fig. 13. Deformation damage of the specimen B2.

the  $1.26f_u$  design value of ordinary steel bolted connection. This finding indicated that high-strength steel under specimen failure could significantly improve utilization efficiency of steel strength. Furthermore, using the design method of ordinary steel connection during joint design would result in partially low computational result.

5.2. Bolt edge distance

Relation curves between bearing capacity and edge distance are shown in Fig. 17, from which it can be realized that edge distance was reduced from  $2.0d_0$  to  $d_0$ , ultimate bearing capacities decreased by 5.9%, 12.3%, and 13.9%, and corresponding deformation capabilities deteriorated by 60.1%, 17.2%, and 27.7%, respectively, when bolts were under transverse arrangement. When bolts were under longitudinal arrangement, edge distance decreased from  $2.0d_0$  to  $d_0$  and ultimate bearing capacities by 44.2%, 39.2%, and 32.0%; therefore, both decrease amplitudes were large. Owing to small edge distance, specimen B7 immediately experienced failure after entering the slippage stage, which showed that edge distance had considerable influence on bearing capacity.

The EC3 standard can reflect the influence of edge distance on load-bearing properties:

When  $e_2 < 1.5d_0$ :

$$\frac{F_b}{f_u dt} = 0.8 \frac{e_1}{3d_0} \left( 2.8 \frac{e_2}{d_0} - 1.7 \right). \tag{18}$$

When  $e_2 \geq 1.5d_0$ :

$$\frac{F_b}{f_u dt} = 0.8 \frac{2.5e_1}{3d_0}. \tag{19}$$

Change curves of specimen-bearing capacity with edge distance are shown in Fig. 17c, which shows that bearing capacity of connections presented a linear growth trend with edge distance. Test results of bolts under longitudinal arrangement were quite approximate to theoretically computed values, and such values were partially low for bolts under transverse arrangement.

Minimum distance was determined when net cross-sectional failure occurred after gross sectional yield, namely:

$$\frac{A_n}{A} \geq \frac{f_y}{f_u}, \tag{20}$$

where  $A_n$  is the net sectional area, and  $A$  is the gross sectional area.

When bolts are under longitudinal arrangement, Eq. (20) can be expressed as:

$$\frac{2-d_0/e_2}{2} \geq \frac{f_y}{f_u}. \tag{21}$$

Eq. (21) shows that edge distance is related to yield strength  $f_y$ , tensile strength  $f_u$ , and bolt hole diameter  $d_0$ . A large yield/strength ratio leads to large edge distance. As yield/strength ratio of Q460D steel was 0.85,  $e_2/d_0 \geq 2$ , which well accorded with the test result, and edge distance was suggested as  $2d_0$ .

5.3. Bolt pitch

Fig. 18 provides change relation curves of bolted connection joint bearing capacities with bolt pitch, which shows that specimen ultimate bearing capacity was reduced as bolt pitch decreased when bolts were under transverse arrangement, and variation trends of curves were relatively approximate. Bolt pitch is reduced from  $3.5d_0$  to  $2.0d_0$ , and

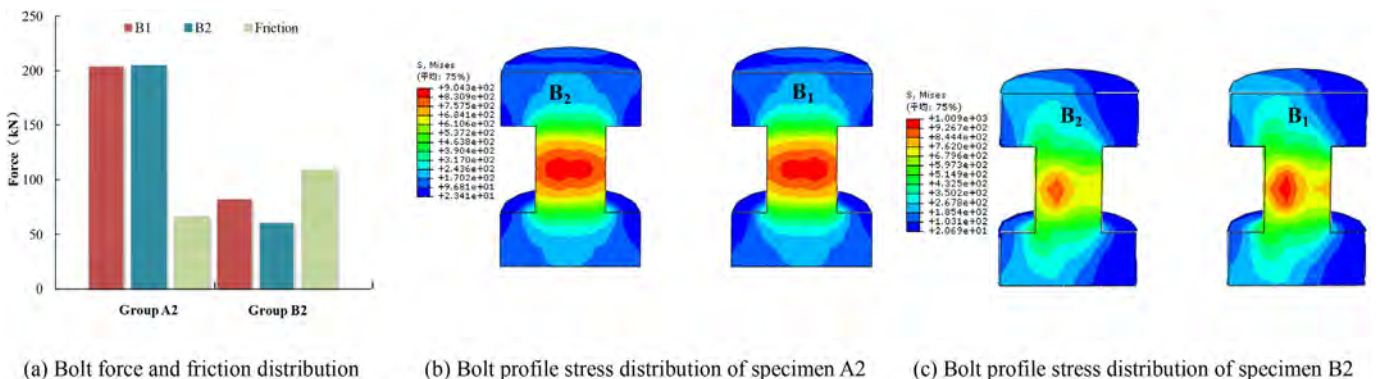


Fig. 14. Bolt contact stress distribution.

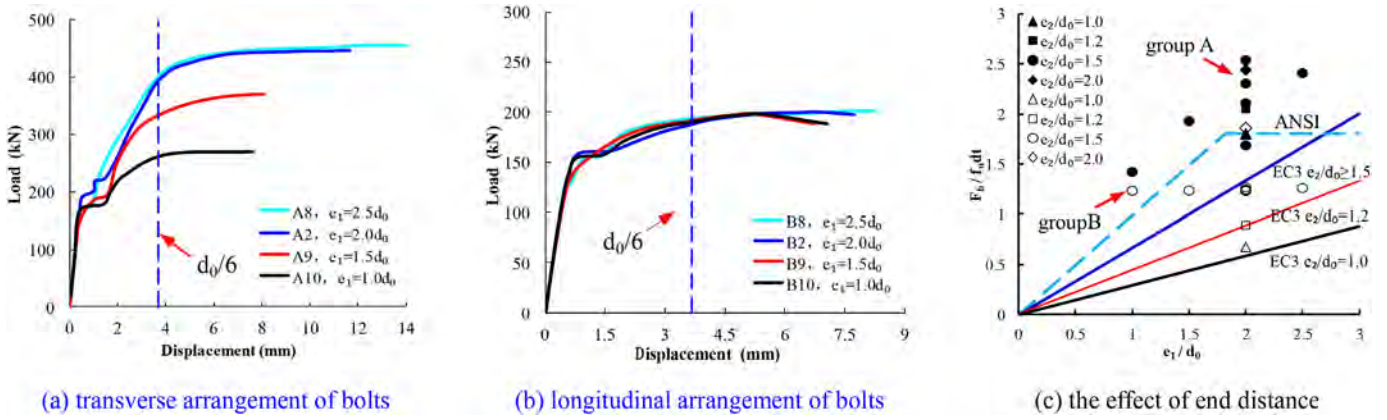


Fig. 15. The effect of end distance.

ultimate bearing capacities decreased by 10.1%, 9.4%, and 25.0%; thus, bolt pitch had a considerable influence on the bearing capacities of bolts under transverse arrangement. When bolts were under longitudinal arrangement, specimen ultimate bearing capacity slightly changed with bolt pitch with change amplitude not exceeding 3.0%. Moreover, initial slippage loads were considerably different, which showed that bolt pitch had a slight influence on bearing capacity when bolts were under longitudinal arrangement.

When bolts were under transverse arrangement, Eq. (20) can be expressed as

$$\frac{(p_2 + 2e_2) - 2d_0}{p_2 + 2e_2} \geq \frac{f_y}{f_u} \quad (22)$$

Based on the preceding equation, edge distance  $e_2$  is suggested as  $2d_0$ , and the following equation can be obtained:

$$1 - \frac{2d_0}{p_2 + 4d_0} \geq \frac{f_y}{f_u} \quad (23)$$

$p_2/d_0 \geq 4$  is obtained according to Eq. (23), and a certain deviation exists with an actual test result. Fig. 18 shows that when bolt pitch increased from  $3d_0$  to  $3.5d_0$ , initial slippage of the specimen, ultimate bearing capacity, and its corresponding deformation with large change amplitudes also increased by 23.9%, 10.1%, and 60.3%, respectively. Therefore, bolt pitch was suggested as  $3.0d_0$ .

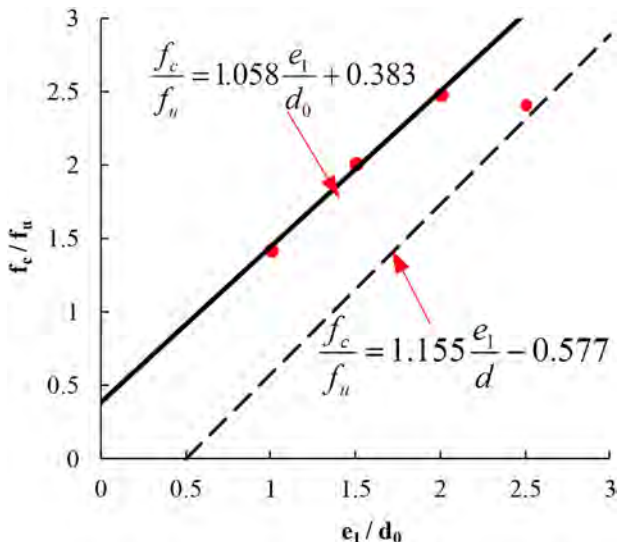


Fig. 16. The end distance-bearing strength curve.

## 6. Theoretical analysis of EC3

Bearing capacity design of pressure-bearing bolted connection is stipulated in EN1993-1-8 [28] as

$$F_{b,Rd} = \frac{k_1 \alpha_b f_u d t}{\gamma_{M2}} \quad (24)$$

where  $F_{b,Rd}$  is the design value of bearing strength at steel plate hole wall,  $\gamma_{M2} = 1.25$ ,  $f_u$  is the tensile strength of steel plate,  $d$  is the bolt diameter, and  $t$  is the thickness of steel plate. Values of parameters  $\alpha_b$  and  $k_1$  should be determined considering the geometric construction, and specific selection refers to the following equation:

In the load transfer direction:

$$\alpha_b = \min \left\{ \alpha_d; \frac{f_{ub}}{f_u}; 1.0 \right\}, \quad (25)$$

where  $\alpha_d$  is taken as  $\frac{e_1}{3d_0}$  and  $\frac{p_1}{3d_0} - \frac{1}{4}$  for end bolt and internal bolt, respectively, and  $f_{ub}$  is the bolt tensile strength.

Perpendicular to the load transfer direction:

For end bolts,

$$k_1 = \min \left\{ 2.8 \frac{e_2}{d_0} - 1.7, 1.4 \frac{p_2}{d_0} - 1.7 \text{ or } 2.5 \right\}, \quad (26)$$

For inner bolts,

$$k_1 = \min \left\{ 1.4 \frac{p_2}{d_0} - 1.7 \text{ or } 2.5 \right\}, \quad (27)$$

where  $e_1 \geq 1.2d_0$ ,  $e_2 \geq 1.2d_0$ ,  $p_1 \geq 2.2d_0$ , and  $p_2 \geq 2.4d_0$ .  $f_{ub}/f_u$  represents the situation in which bolt material strength is lower than that of steel, while the absence of shear failure in the bolt can be ensured during the design process.

Moze [10] indicates that the formula of bearing capacity in EC3 is partially conservative in a few failure models, and the total sum of single bolt bearing capacities does not represent the maximum bearing capacity of connections. Verification was carried out in consideration of relations among ultimate load, net cross-section failure, tear-out failure and shear failure, and net cross-section design referred to in EN1993-1-12 [35]:

$$N_{t,Rd} = \frac{0.9 A_{net} f_u}{\gamma_{M12}}, \quad (28)$$

where  $N_{t,Rd}$  is the design bearing capacity of net cross section,  $A_{net}$  is the net cross-section area, and  $\gamma_{M12} = 1.25$ .

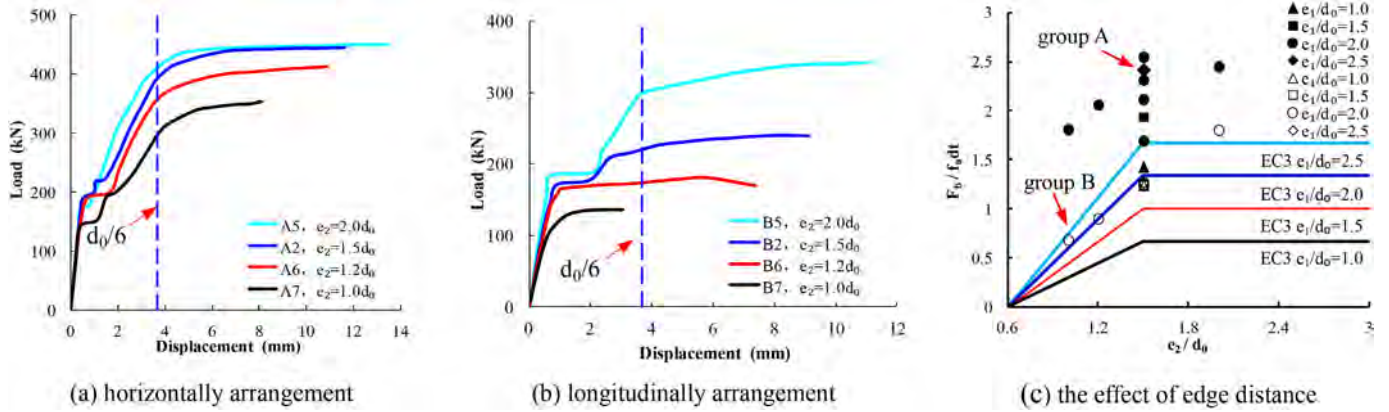


Fig. 17. The effect of edge distance.

Blocking tearing was mostly shear failure of bolts along hole wall, and diagonal cracks were generated between screw holes under tensile stress. Block tearing resistance  $V_{eff,1,Rd}$  referred to in EN1993-1-8 definition in the European standard is as follows:

$$V_{eff,1,Rd} = \frac{A_{nt}f_u}{\gamma_{M_2}} + \frac{A_{nv}f_y}{\gamma_{M_0}\sqrt{3}} \quad (29)$$

where  $V_{eff,1,Rd}$  is the design bearing capacity of block tearing;  $A_{nt}$  and  $A_{nv}$  are tensile and shear-bearing net sectional areas, respectively;  $\gamma_{M_0} = 1.1$ ;  $f_y$  is yield strength; and  $f_u$  is tensile strength of steel plate.

The relationships between bolt bearing capacity and standard computed value in groups A and B specimens are shown in Fig. 19. Bolts in group A under transverse arrangement were distributed along load transfer direction and stresses borne by end bolts  $B_1$  and  $B_2$  were identical. Based on fitting curves and data point dispersion degree in Fig. 19a and b, deviation was large when EC3 formula was used to estimate bearing capacities of bolt specimens under transverse arrangement, and bearing capacities of connection joints were usually underestimated.

Bolts  $B_1$  and  $B_2$  bore different stresses in group B specimens; hence, stress distribution of connecting plate was not uniform. Fig. 19a and b show that the distribution of inner bolt  $B_2$  was relatively dispersed compared with that of end bolt  $B_1$ . From fitting curves and data point distribution, bolt  $B_1$  was approximate to the EC3 computed value. However, fitting curve slopes of specimens under longitudinal arrangement were all smaller than those under transverse arrangement higher than the limiting value of the EC3 standard. When connection bearing capacity was expressed by the total sum  $\sum F_b$  of single bolts, specimens under

transverse arrangement had higher margin than those under longitudinal arrangement. Moreover, ultimate load of the connection was not completely equal to the sum of bearing capacities of all bolts due to the influence of friction force on steel plate surface to a certain degree.

Table 5 shows that ultimate bearing capacities of bolts under transverse arrangement were all larger than those under longitudinal arrangement. Specimens under transverse arrangement presented an increasing bearing capacity trend as end and edge distance increased; for bolts under longitudinal arrangement, end distance and pitch had slight influences on ultimate bearing capacity. Finite element numerical points in Fig. 19e were distributed to both sides of the dotted line, and the difference between computed value and test value was within 10%. Therefore, goodness of fit was very high, and basic load-bearing properties of connections could be accurately reflected.

### 7. Conclusions

Influences of parameters, such as bolt arrangement pattern and joint construction on mechanical properties of connection joints, were discussed based on an experimental study of the properties of Q460D high-strength steel bolted connections. The following conclusions could be obtained:

- 1) Failure mode and bearing capacity of bolted connection joints were closely related to bolt arrangement pattern and structural form. An equation was established according to force equilibrium and deformation coordinating conditions. The difference value between initial

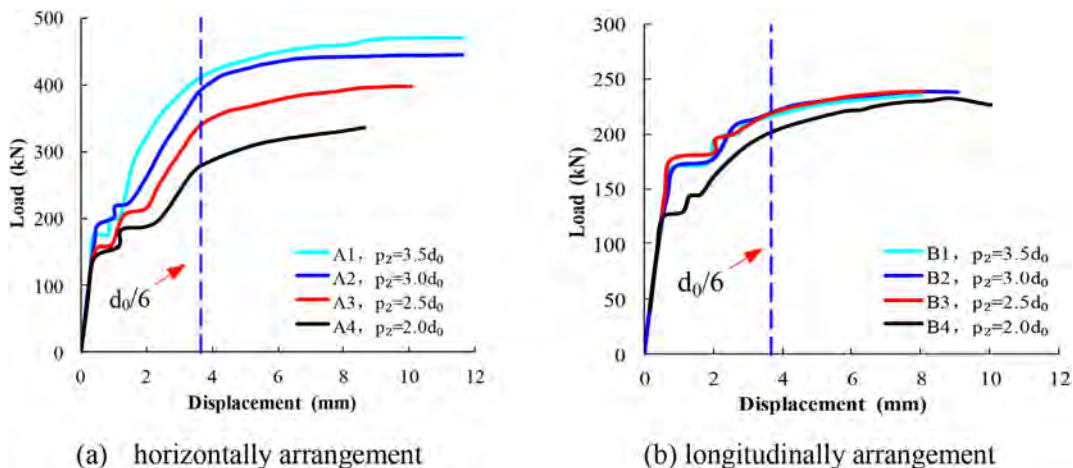


Fig. 18. The effect of bolt pitch.

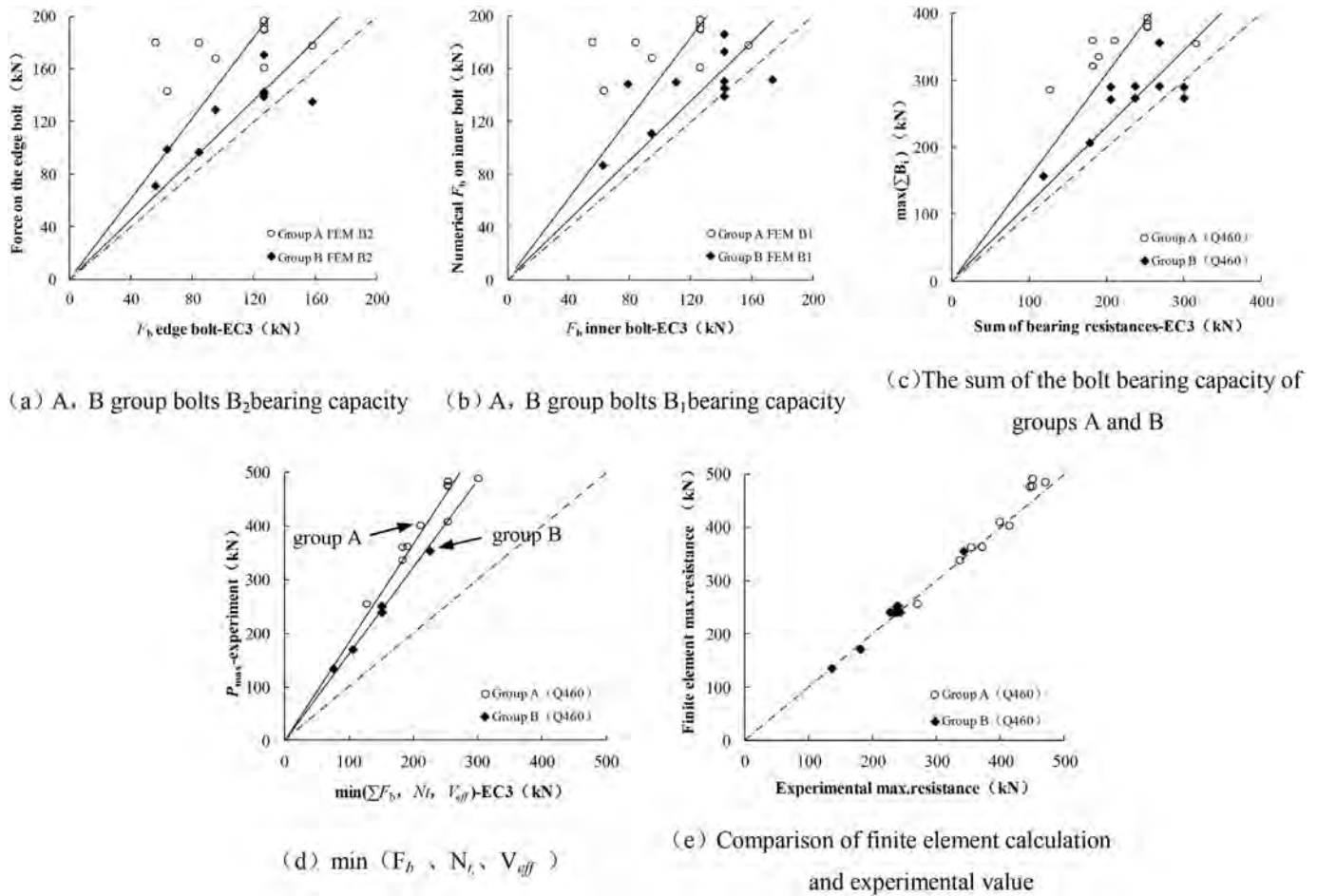


Fig. 19. The comparison of bolt bearing capacity.

slippage load obtained through theoretical computation and test value did not reach 4% with favorable applicability.

- 2) When bolts were under transverse arrangement, specimen bearing capacity presented a linear growth with end distance, edge distance, and bolt pitch; fitting trend through ANSI standard was quite approximate while the EC3 standard was partially conservative. When bolts were under longitudinal arrangement, net cross-section capacity of the connection only presented a linear growth trend as edge distance increased, influence ranges of end distance and bolt pitch did not exceed 3%, and the EC3 standard had improved fitting effect.
- 3) Finite element model coincided with test results very well in reflecting specimen stress distribution, failure mode, and bearing capacity. When displacement value was  $d_0/6$ , bearing capacity

could reach over 85% of ultimate bearing capacity, and difference value between test value and numerical analysis result was within 10%.

- 4) When bolts were under transverse arrangement, two bolt holes bore relatively uniform stresses, and stress nephogram and plastic region were under symmetrical distribution; when bolts were under longitudinal arrangement, two holes bore non-uniform stresses, and end bolt holes bore large stress and experienced large deformation.
- 5) For Q460D steel, the deviation was large when the EC3 standard formula was used to compute bearing capacities of bolts under transverse arrangement; for bolt specimens under longitudinal arrangement, computational effects of end bolts and inner bolts were satisfactory.

Table 5  
Bearing capacity of specimen.

Specimen number	$B_1$ (kN)	$B_2$ (kN)	Friction (kN)	$\max(\sum B_i)$ (kN)	$P_{max}$ (kN)	Specimen number	$B_1$ (kN)	$B_2$ (kN)	Friction (kN)	$\max(\sum B_i)$ (kN)	$P_{max}$ (kN)
A1	194.64	197.17	93.08	391.82	484.89	B1	101.43	70.08	68.86	171.51	240.37
A2	204.11	205.11	67.25	409.22	476.47	B2	81.08	60.71	110.24	141.79	252.03
A3	193.94	174.74	41.53	368.69	410.22	B3	113.37	58.55	68.91	171.92	240.83
A4	127.28	131.14	79.66	258.42	338.08	B4	112.25	46.82	81.58	159.08	240.66
A5	190.56	191.65	95.04	382.22	477.26	B5	119.18	76.75	159.00	195.93	354.93
A6	141.67	115.91	145.43	257.58	403.01	B6	81.06	54.81	35.17	135.87	171.04
A7	131.00	101.57	129.92	232.57	362.49	B7	67.41	41.75	25.67	109.16	134.83
A8	169.54	164.75	156.56	334.29	490.85	B8	84.30	55.46	100.61	139.76	240.37
A9	99.54	106.25	157.71	205.79	363.50	B9	93.16	59.61	87.56	152.76	240.32
A10	103.37	104.18	48.85	207.55	256.40	B10	98.28	54.19	98.89	152.47	251.36

## Acknowledgment

The authors would like to thank the financial support of the National Natural Science Foundation of China No. 51308454 and the State Key Laboratory Base of Eco-hydraulic Engineering in Arid Area No. 2017ZZKT-8.

## References

- [1] S. Responsables, Use and Application of High-Performance Steels for Steel Structures, IABSE-AIPC-IVBH, Zürich, Switzerland, 2005.
- [2] R. Bjorhovde, Development and use of high performance steel, *J. Constr. Steel Res.* 60 (3) (2004) 393–400.
- [3] R. Bjorhovde, Performance and design issues for high strength steel in structures, *Adv. Struct. Eng.* 13 (3) (2010) 403–411.
- [4] I.H. Kim, S.H. Cho, J.H. Kim, et al., Economic evaluation of high-strength steel for structural member types in building structures, *J. Comput. Struct. Eng. Inst. Korea* 26 (2) (2013) 113–121.
- [5] J.J. Wallaert, J.W. Fisher, Shear strength of high-strength bolts, *J. Struct. Div.* 91 (3) (1965) 99–126.
- [6] J.W. Fisher, Behavior of fasteners and plates with holes, *J. Struct. Div.* 91 (6) (1965) 265–286.
- [7] Y. Zeynali, M.J. Samimi, A. Mazroi, J.A. Marnani, M.S. Rohanimanesh, Experimental and numerical study of frictional effects on block shear fracture of steel gusset plates with bolted connections, *J. Thin-Walled Struct.* 121 (9) (2017) 8–24.
- [8] E.J. Pavlina, C.J. Vantyne, Correlation of yield strength and tensile strength with hardness for steels, *J. Mater. Eng. Perform.* 17 (6) (2008) 888–893.
- [9] P. Dusicka, G. Lewis, High strength steel bolted connections with filler plates, *J. Constr. Steel Res.* 66 (1) (2010) 75–84.
- [10] Primoz Moze, Darko Beg, High strength steel tension splices with one or two bolts, *J. Constr. Steel Res.* 66 (8) (2010) 1000–1010.
- [11] Primoz Moze, Darko Beg, Investigation of high strength steel connections with several bolts in double shear, *J. Constr. Steel Res.* 67 (3) (2011) 333–347.
- [12] Primoz Moze, Darko Beg, A complete study of bearing stress in single bolt connections, *J. Constr. Steel Res.* 95 (95) (2014) 126–140.
- [13] G.H. Sterling, J.W. Fisher, A440 steel joints connected by A490 bolts, *J. Struct. Div. Am. Soc. Civil Eng.* 92 (3) (1966) 304–305.
- [14] Y. Shi, B. Pan, G. Shi, et al., Experimental study on high strength steel plate bolted connections under shear force, *J. Ind. Constr.* 42 (1) (2012) 56–61 (in Chinese).
- [15] T.S. Kim, H. Kuwamura, Numerical investigation on strength design and curling effect of mechanically fastened joints in cold-formed austenitic stainless steel, *J. Mater. Des.* 32 (7) (2011) 3942–3956.
- [16] T.S. Kim, H. Kuwamura, Finite element modeling of bolted connections in thin-walled stainless steel plates under static shear, *J. Thin-Walled Struct.* 45 (4) (2007) 407–421.
- [17] R. Puthli, O. Fleischer, Investigations on bolted connections for high strength steel members, *J. Constr. Steel Res.* 57 (3) (2001) 313–326.
- [18] A. Aalberg, P.K. Larsen, Strength and ductility of bolted connections in normal and high strength steels, Norwegian University of Science and Technology, Trondheim, 1999.
- [19] A. Aalberg, P.K. Larsen, Bearing strength of bolted connections in high strength steel, Proceedings of Nordic Steel Construction Conference, 2001.
- [20] C.O. Rex, W.S. Easterling, Behavior and modeling of a bolt bearing on a single plate, *J. Struct. Eng.* 129 (6) (2003) 792–800.
- [21] G. Liang, H.C. Guo, Y.H. Liu, et al., Q690 high strength steel T-stub tensile behavior: experimental and numerical analysis, *J. Thin-Walled Struct.* 122 (2018) 554–571.
- [22] H.C. Guo, G. Liang, Y.H. Liu, et al., Q690 high strength steel T-stub tensile behavior: experimental research and theoretical analysis, *J. Constr. Steel Res.* 139 (2017) 473–483.
- [23] E.J. Pavlina, C.J.V. Tyne, Correlation of yield strength and tensile strength with hardness for steels, *J. Mater. Eng. Perform.* 17 (6) (2008) 888–893.
- [24] P. Langenberg, Relation between design safety and Y/T ratio in application of welded high strength structural steel in, Proceedings of International Symposium on Application of High Strength Steels in Modern Constructions and Bridges-Relationship of Design Specifications, Safety and Y/T Ratio, Beijing, China 2008, pp. 28–46.
- [25] GB50017-2017, Code for Design of Steel Structure, China Planning Press, Beijing, 2017 [in Chinese].
- [26] BS EN1993-1-8, Eurocode 3: Design of Steel Structure-Part 1-8: Design of Joints, European Committee for Standardisation, Brussels, 2005.
- [27] ANSI/AISC 360-05, Specification for Structural Steel Buildings, American Institute of Steel Construction, 2005.
- [28] JGJ82-2011, Technical Specification for High Strength Bolt Connect of Steel Structure, China Building Industry Press, Beijing, 2011 [in Chinese].
- [29] GB/T228-2002, Metallic Materials-Tensile Testing at Ambient Temperature, China Standard Press, Beijing, 2002 [in Chinese].
- [30] GB/T2975-1998, Steel and Steel Products-Location and Preparation of Test Pieces for Mechanical Testing, China Standard Press, Beijing, 1999 [in Chinese].
- [31] GB/T228.1-2010, Metallic Materials-Tensile Testing-Part 1: Method of Test at Room Temperature, China Standard Press, Beijing, 2012 [in Chinese].
- [32] Y. Wang, H. Chen, Y. Shi, et al., High Strength Bolted Joints, China Railway Publishing House, Beijing, 1984 151–158 (in Chinese).
- [33] BS EN1993-1-12, Eurocode 3: Design of Steel Structures-Part 1-12: Additional Rules for the Extension of EN 1993 Up to Steel Grades S700, European Committee for Standardisation, Brussels, 2007.
- [34] B. Pan, Y. Shi, Y. Wang, Finite element analysis of bolted connection in Q460 grade high strength steels under static shear, *J. Archit. Civil Eng.* 29 (2) (2012) 48–54 (in Chinese).